Journal of Physics: Conference Series

PAPER • **OPEN ACCESS**

Flow around a low-aspect-ratio wall-bounded 2D hydrofoil: a LES/PIV study

Flow around a low-aspect-ratio wall-bounded 2D hydrofoil: a LES/PIV study

E I Dauengauer[1,2], R I Mullyadzhanov[1,2], M V Timoshevskiy[1], I I Zapryagaev[1], K S Pervunin[1]

[1] Institute of Thermophysics SB RAS, 1 Lavrentyev Ave., 630090 Novosibirsk, Russia
[2] Novosibirsk State University, 1 Pirogov Str., 630090 Novosibirsk, Russia

E-mail: edauengauer@mail.ru

Abstract. We performed Large-eddy simulations (LES) of the flow around a low-aspect-ratio wall-bounded 2D hydrofoil at the zero angle of attack using spectral-element method (SEM). The flow was considered for several Reynolds numbers Re_C = 500, 5.0×10^3, 5.0×10^4 and 1.2×10^6 based on the foil chord to reveal the influence of the test channel sidewalls and viscous effects. The laminar-turbulent transition of the boundary layer was registered. A comparison of the numerical results with experimental data for the highest Reynolds number was performed and showed an excellent agreement.

1. Introduction

Flow around bluff bodies and wings has long been the subject of extensive research due to its practical relevance for airspace and (under)water transport and turbomachinery, being an example of a complex flow featuring separation and accompanying phenomena. The separation is usually connected to the laminar-turbulent transition of a boundary layer (BL), BL evolution under the influence of an adverse pressure gradient, formation of a recirculating zone affecting the ambient pressure field and, as a result, leading to variations of the forces acting on a body. Previous studies cover different aspects of separated flows over foils which are also considered in many comprehensive reviews and textbooks [1–4]. With the rapid growth of computational resources over the past few decades, large-scale numerical simulations have become a widely spread and effective tool to predict flow dynamics in complex configurations. Jansen [5] performed Large-eddy simulations (LES) of the flow around a NACA4412 profile for the Reynolds number $\mathrm{Re}_C = 1.64\times10^6$ based on the hydrofoil chord length C, comparing the numerical results with available experimental data [6–8]. Direct numerical simulations (DNS) of the flow about a NACA0012 section at different angles of attack were carried out by Shan et al. [9] for $\mathrm{Re}_C = 1.0\times10^5$, Rodríguez et al. [10] for $\mathrm{Re}_C = 5.0\times10^4$ and recently by Hosseini et al. [11] for $\mathrm{Re}_C = 4.0\times10^5$. Serson et al. [12] and Munday et al. [13] studied the effect of surface geometry modification and active mass injections to improve the lift-drag ratio of a wing. Another topical issue is simulation of cavitating flow that was conducted, for instance, by Wang and Ostoja-Starzewski [14] and Ji et al. [15] for NACA0015 and NACA66 hydrofoils, respectively. Despite thorough investigations in this particular field, the problem in general remains unsolved and is still important and urgent. In this paper, we report on preliminary results of LES computations of the subcavitating flow around a scaled-down model of guide vanes (GV) of a Francis turbine mounted in a rectangular channel at zero angle of attack ($\alpha = 0°$) for different Reynolds numbers and then compare them with the ones of PIV measurements [16]. The research is motivated by the need to reveal the effect of

IOP Conf. Series: Journal of Physics: Conf. Series **1128** (2018) 012085 doi:10.1088/1742-6596/1128/1/012085

sidewalls on cavitation onset, transition to unsteady regimes and partial cavity characteristics on movable operating elements of hydraulic equipment.

2. Computational method and boundary conditions

We performed Large-eddy simulations (LES) of the single-phase flow around a low-aspect-ratio 2D hydrofoil representing a scaled-down model of guide vanes (GV) of a Francis turbine, with the geometry described in [16]. We use the computational code Nek5000 [17] based on the spectral-element method and previously validated in a number of case studies [18–20]. The incompressible Navier–Stokes equations

$$\frac{\partial \vec{u}}{\partial t} = -(\vec{u}\nabla)\cdot\vec{u} + \nu\Delta\vec{u} - \frac{1}{\rho}\nabla p, \qquad \nabla\cdot\vec{u} = 0 \tag{1}$$

are solved in the computational domain which is divided into elements, where the velocity and pressure fields are approximated by high-order Lagrange polynomials. These polynomials are based on the Gauss–Lobatto–Legendre rule

$$u = \sum_{l=1}^{N} a_l \Psi_l(x), \qquad \Psi_l(x) = \prod_{l\neq j}^{N} \frac{x - x_j}{x_l - x_j}, \tag{2}$$

where a_l are the coefficients of expansion, $\Psi_l(x)$ are the N-order Lagrange polynomials. For the time discretization, an implicit third-order backward differentiation formula (k = 3) is used

$$\frac{\partial u^{(n+1)}}{\partial t} = \sum_{j=0}^{k} \frac{b_j}{\Delta t} u^{(n+1-j)}, \tag{3}$$

where $b_0 = \frac{11}{6}$, $b_1 = -\frac{18}{6}$, $b_2 = \frac{9}{6}$ and $b_3 = -\frac{2}{6}$, Δt is the constant time step.

In this study, four Reynolds numbers are considered $\mathrm{Re}_C = CU_0/\nu$ = 500, 5.0×10^3, 5.0×10^4 and 1.2×10^6, where C = 100 mm is the hydrofoil chord length and U_0 is the mean velocity of the incoming flow. The foil angle of attack is α = 0º for all the cases. The computational domain fully corresponds to the test rectangular channel of the experimental rig in the Institute of Thermophysics [21]. Two-dimensional slices of the computational domain together with the coordinate system are presented in figure 1, where x, y and z are the coordinates along the streamwise, transversal and spanwise directions, respectively. The hydrofoil maximum thickness D = 21.4 mm is used as a typical lengthscale. The hydrofoil span dimension is roughly 3.7D and matches the width of the rectangular channel, with its cross-section being $y\times z$ = 11.7$D\times$3.7D. The channel length in the x-direction is 30.5D. The hydrofoil chord length is C = 4.67D. Details of the computational mesh are given in table 1 and its visualization is shown in figure 2. Inflow parameters for the velocity field are set according to the experimental measurements [16] with a uniform flow in the central part of the channel and relatively thin boundary layers near walls, where the no-slip condition is applied. The outflow boundary condition corresponds to the Neumann condition. We performed Large-eddy simulations (LES) of equations (1). The subgrid-scale model is not used assuming a sufficient spatial resolution, while two high-frequency modes are filtered applying a parabolic transfer function with amplitude of 5% for the latter mode [22].

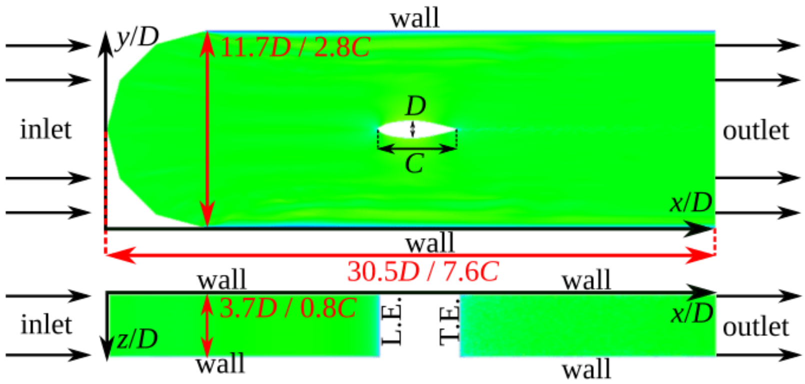

Figure 1. Slice of the computational domain in the x-y plane (up) and in the x-z plane (bottom). D and C are the GV maximum thickness and chord length. L.E. and T.E. stand for the leading and trailing edges of the hydrofoil.

Table 1. Mesh characteristics of the whole computational domain and around the hydrofoil. The number of nodes equals the number of spectral elements (SE) multiplied by N^3. For higher and lower Re_C, N = 8 and 6, respectively.

Re_C	SE	Nodes	on the hydrofoil	
			SE	Nodes
500, 5.0×10^3, 5.0×10^4	38304	8273664	768	165888
1.2×10^6	140448	71909376	2816	1441792

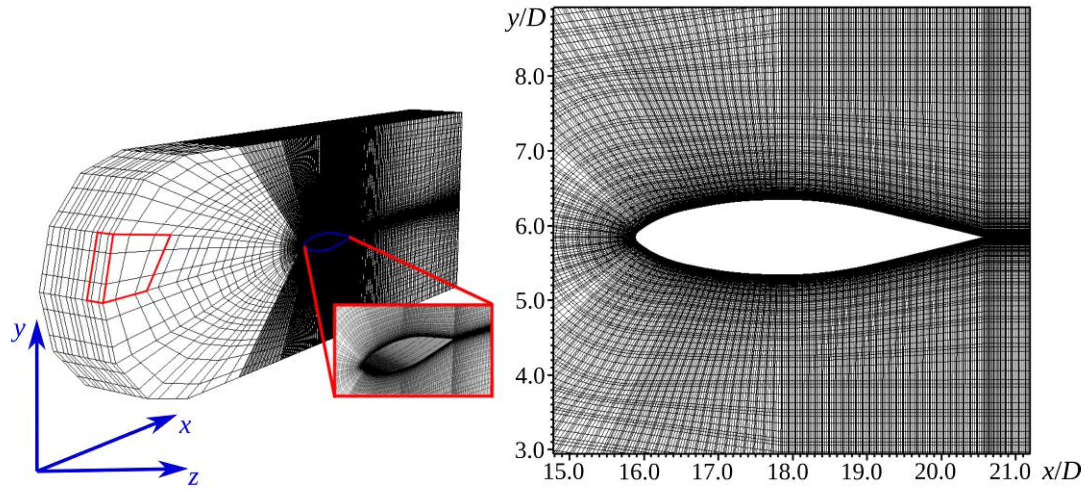

Figure 2. Computational domain (left) and near-hydrofoil blow up of a two-dimensional slice in the *x*-*y* plane (right). $\mathrm{Re}_C = 1.2\times10^6$.

3. Results

The two-dimensional visualization of velocity and pressure fields in figure 3 demonstrates a decrease in the BL thickness and intensification of turbulence level of the separated mixing layer with an increase of Re_C. At the lowest Reynolds number (Re_C = 500), the simulations display that the flow is steady while for $\mathrm{Re}_C = 5.0\times10^3$ the wake becomes unsteady at roughly x/D = 22. A further increase of the Reynolds number to $\mathrm{Re}_C = 5.0\times10^4$ leads to the boundary layer (BL) turbulization already at $x/D \approx$ 19. When the Reynolds number is indeed high ($\mathrm{Re}_C = 1.2\times10^6$) and very close to the experimental one, BL becomes extremely thin and undergoes the turbulent transition in the aft part of the GV model (x/D = 19.5–20) but the wake behind the hydrofoil trailing edge is very narrow and weak. The pressure fields along the GV model are quite typical for all Reynolds numbers, with the maximum located around the foil leading edge. Halfway along the surface, the local pressure reaches its minimum value due to the flow acceleration and further downstream it increases again. However, the vortical pattern is conveniently reflected in the pressure field only for $\mathrm{Re}_C = 5.0\times10^4$, indicating relatively strong eddies. Figure 4 shows the effect of viscosity or Reynolds number on the BL evolution and the mean velocity profile along the *x*-coordinate. As seen, at lower Re_C the velocity profile tends to the Poiseuille solution relatively fast, while, for higher Re_C, it does not change noticeably. A rapid increase of the velocity magnitude right after the leading edge occurs due to the flow acceleration over the hydrofoil. Downstream evolution of the mean velocity in a close-to-wall region above the GV model is shown in figure 5 for all Re. As seen, a growth of the Reynolds number results in a reduction of the relative velocity magnitude causing a strong difference between all these cases. The numerical results are justified by an excellent agreement with the experimental data at $\mathrm{Re}_C = 1.2\times10^6$ (figure 5).

4. Conclusions

Using Large-eddy simulations we studied the single-phase flow around a scaled-down model of guide vanes (GV) of a Francis turbine mounted in a rectangular test channel. The instantaneous velocity and pressure fields around the GV model were analyzed together with the profiles of the time-averaged velocity for Reynolds numbers Re_C = 500, 5.0×10^3, 5.0×10^4, 1.2×10^6. The laminar-turbulent transition of the boundary layer was registered. For $\mathrm{Re}_C = 1.2\times10^6$, an excellent agreement between the numerical results and experimental data was obtained.

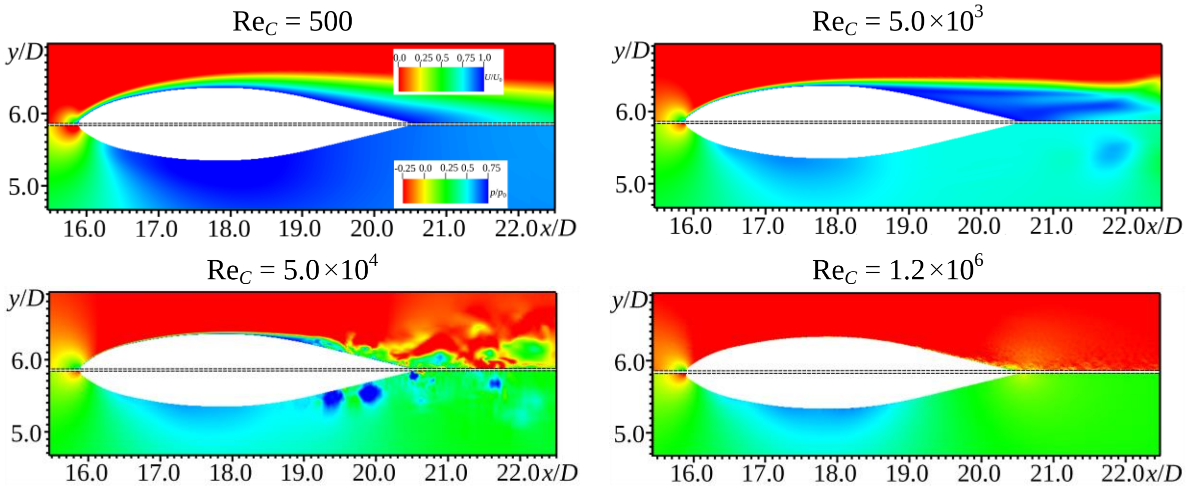

Figure 3. Instantaneous streamwise velocity (top) and pressure (bottom) fields near the GV model in the middle *x*-*y* section of the test channel (z/D = 1.85) for different Reynolds numbers. The flow direction is from the left.

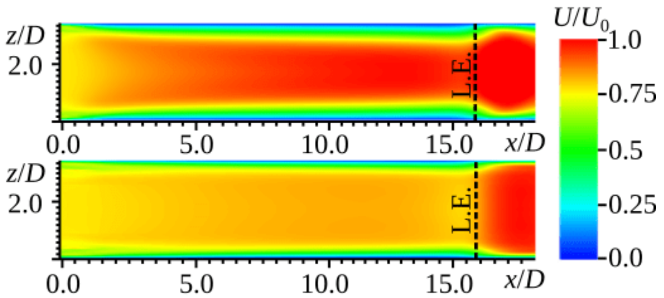

Figure 4. 2D distributions of the streamwise component of the mean velocity in the *x*-*z* plane (y/D = 6.8) for Re_C = 500 (top) and 5.0×10^3 (bottom). The dotted black line denotes the GV leading edge. The flow direction is from the left.

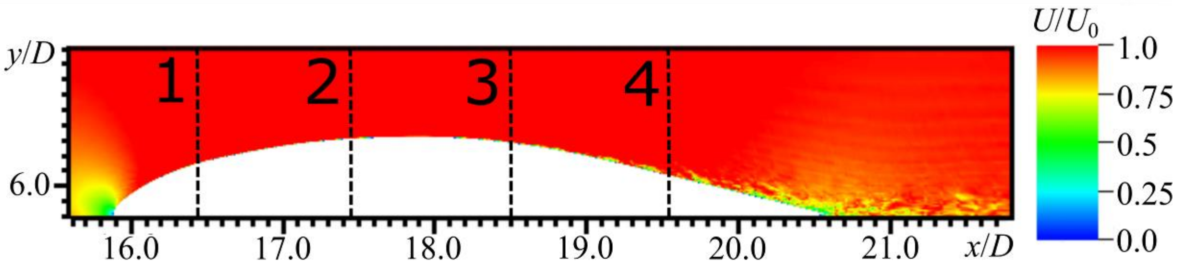

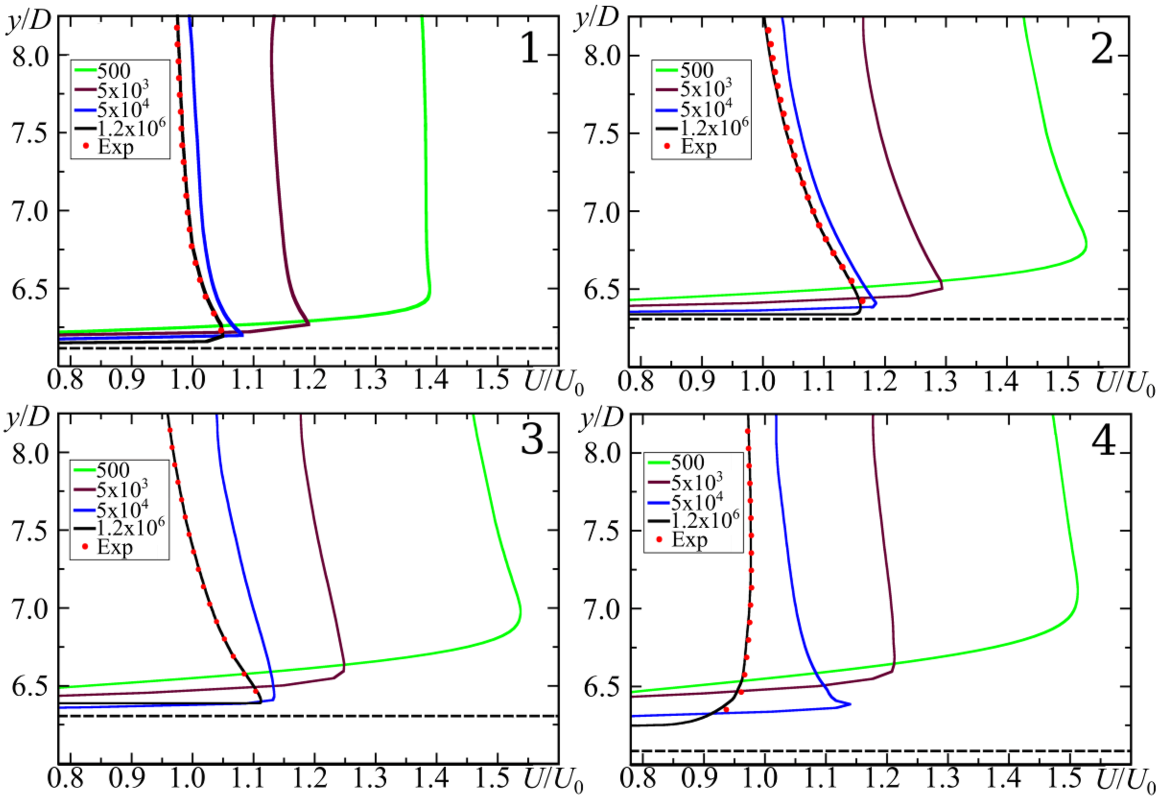

Figure 5. Profiles of the streamwise component of the time-averaged velocity over the hydrofoil in the median longitudinal plane of the test channel for all Reynolds numbers (lines) in comparison with the experimental data [16] (symbols) in several cross-sections indicated in the scheme above: (1) x/D = 16.45, (2) 17.45, (3) 18.5 and (4) 19.55. Dashed black line denotes the hydrofoil surface. The flow direction is from the left.

Acknowledgments
The research was funded by the Russian Foundation for Basic Research (Project No. 18-38-00907) and the Ministry of Science and Higher Education of the Russian Federation (Project No. III.22.7.1). The computational resources were provided by the Siberian Supercomputer Center SB RAS, the Novosibirsk State University Supercomputer Center and the Joint Supercomputer Center RAS.

References
[1] Dennis S C R and Chang G-Z 1970 *J. Fluid Mech.* **42(3)** 471–489
[2] Simpson R L 1989 *Ann. Rev. Fluid Mech.* **21(1)** 205–232
[3] Simpson R L 1996 *Prog. Aerosp. Sci.* **32(5)** 457–521
[4] Tobak M and Peake D J 1982 *Ann. Rev. Fluid Mech.* **14(1)** 61–85
[5] Jansen K. 1996 *Ann. Res. Briefs* 225–232
[6] Coles D and Wadcock A J 1979 *AIAA J* **17(4)**, 321–329
[7] Hastings R C and Williams B R 1987 *Aeronaut J* **91(901)** 29–44
[8] Wadcock A J 1987 *Investigation of low-speed turbulent separated flow around airfoils* (Moffett Field California: NASA Technical Reports) p 66
[9] Shan H, Jiang L and Liu C 2005 *Comp. Fluids* **34(9)** 1096–1114
[10] Rodríguez I, Lehmkuhl O, Borrell R and Oliva A 2013 *Int. J. Heat Fluid Flow* **43** 194–203
[11] Hosseini S M, Vinuesa R, Schlatter P, Hanifi A and Henningson D S 2016 *Int. J. Heat Fluid Flow* **61** 117–128
[12] Serson D, Meneghini J R and Sherwin S J 2017 *Comp. Fluids* **146** 117–124
[13] Munday Ph M and Taira K 2018 *AIAA J.* **56(5)** 1830–1842

[14] Wang G and Ostoja-Starzewski M 2007 *Appl. Math. Model.* **31(3)** 417–447
[15] Ji B, Luo X W, Arndt R E A, Peng X and Wu Y 2015 *Int. J. Multiphase Flow* **68** 121–134
[16] Timoshevskiy M V, Churkin S A, Kravtsova A Yu, Pervunin K S, Markovich D M and Hanjalić K 2016 *Int. J. Multiphase Flow* **78** 75–87
[17] Fischer P, Kruse J, Mullen J, Tufo H, Lottes J and Kerkemeier S 2008 *Nek5000: open source spectral element CFD solver* (Argonne Illinois: Argonne National Laboratory, Mathematics and Computer Science Division, https://nek5000.mcs.anl.gov)
[18] Ryzhenkov V, Ivashchenko V, Vinuesa R and Mullyadzhanov R 2016 *J. Phys. Conf. Ser.* **754(6)** (062009)–7
[19] Ryzhenkov V, Ivashchenko V, Vinuesa R and Mullyadzhanov R 2017 *EPJ Web Conf.* **159** (00041)–5
[20] Ryzhenkov V and Mullyadzhanov R 2017 *J. Phys. Conf. Ser.* **899(2)** (022014)–6
[21] Kravtsova A Yu, Markovich D M, Pervunin K S, Timoshevskiy M V and Hanjalić K 2014 *Int. J. Multiphase Flow* **60** 119–134
[22] Marin O, Vinuesa R, Obabko A V and Schlatter P 2016 *Phys. Fluids* **28(12)** (125101)–26